

Path re-planning method for an AUV to image rough terrain by on-site quality evaluation

Ayaka Kume, Toshihiro Maki, Takashi Sakamaki, Tamaki Ura

The University of Tokyo

Meguro, Tokyo, 153-8505 Japan

{kume,maki,ura}@iis.u-tokyo.ac.jp

Abstract—Although autonomous underwater vehicles(AUVs) are suitable for seafloor imaging, it is currently difficult for them to evaluate the results on-site. Therefore the obtained image map often has omissions caused by occlusions, disturbance, and so on. In order to improve the coverage of the map, operators have to plan new path and then deploy the AUV again. It is quite time-consuming and troublesome. The authors propose a method for an AUV to obtain a full-coverage 3D image of rough seafloor with single deployment. First, an AUV observes the seafloor by following a pre-determined path. Second, the AUV calculates the following things on site based on the obtained data: 3D bathymetry map, uncovered areas on the map, and the next path which can image the uncovered areas effectively. Then, the AUV follows the new path to obtain better results. The performance of this method was verified by tank experiments using the AUV Tri-TON and discuss about precision.

I. INTRODUCTION

Although acoustic observation is mainly performed for seafloor measurement, visual observation is required when high resolution or color information is necessary. In fact, visual observation is used at the exploration of hydrothermal deposit, which attracts attention in terms of mineral resources. As autonomous underwater vehicles (AUVs) can be operated fully automatically, they can observe large area effectively. In fact, many AUVs are used for visual observation. AUV Sirius are used for observation of Great Barrier Reef [1], [2]. AUV Tri-Dog1 observed tube worm colony at Tagiri vent field, Kagoshima Bay in Japan [3]. As a conventional AUV for imaging has downward camera and follows a pre-determined path, the obtained image map often has omissions caused by occlusions, disturbance and so on. Especially, vertical walls cannot be observed at all. In that case the operators have to find out the omissions, plan the new path to observe them and deploy the AUV again. It is quite time-consuming and troublesome. So the authors propose a method for AUVs to obtain a full-coverage 3D image of rough seafloor with single deployment. The performance of this method was verified by tank experiments using the AUV Tri-TON.

II. METHOD

There are three prerequisites for the proposed method:

- The vehicle is a hovering type AUV which can move in surge, sway, and heave direction and make a pivot turn.
- The vehicle has at least one camera and sensor for measuring terrain.

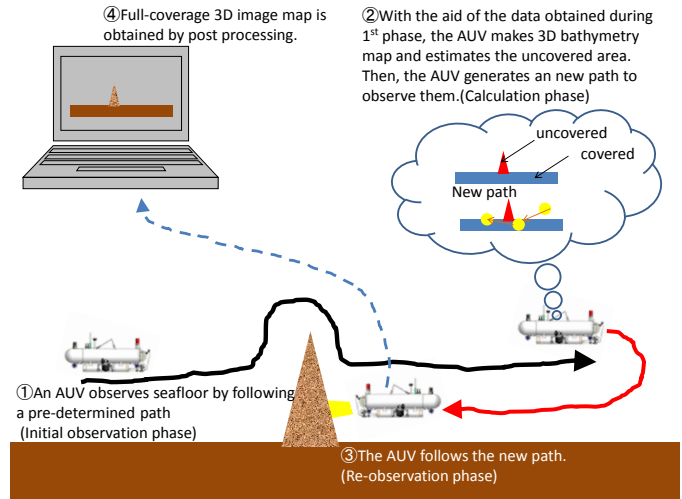


Fig. 1. Outline of the method

- The vehicle is capable of obstacle avoidance and self-location.

The outline of the method is shown in Fig.1. First, an AUV observes the seafloor by following a pre-determined path such as lawn mower pattern (① Initial observation phase). Second, the AUV calculates the following things on-site based on the obtained data (② Calculation phase):

- 3D bathymetry map (Section III-A)
- uncovered areas on the map (Section III-B)
- the next path to image the uncovered areas effectively (Section IV)

Then, the AUV follows the new path to obtain better results (③ Re-observation phase). At last, the full coverage 3D image map is obtained(④ Post processing).

III. MESH EVALUATION

A. Mesh generation

Fig. 2 shows the outline of the mesh generation. 3D triangulated mesh representing the seafloor is constructed using point cloud obtained by initial observation. First, noise is removed from the point cloud by Sun's method [4] and the spatial relations among the points. Second, 3D triangulated mesh is constructed by Delaunay triangulation [5]. Then, the vertexes are reduced by Quadric error metrics [6]. At last, the

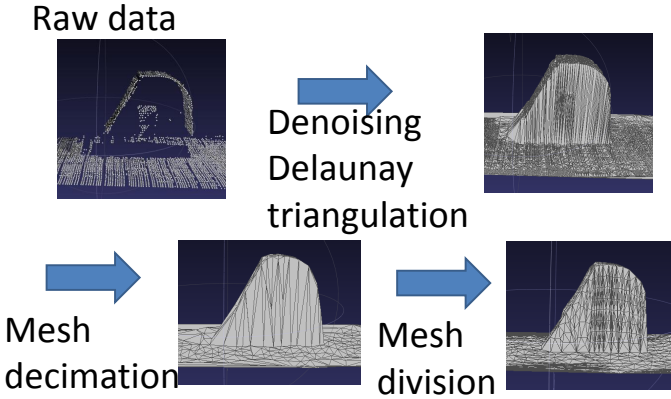


Fig. 2. Outline of mesh generation

edges longer than threshold is divided in order to make sure that each mesh is small enough to be captured in a image.

B. Mesh evaluation

Fig.3 gives an outline of the mesh evaluation method. The method judges whether of not each mesh is covered , based on the images themselves and the position of the camera at the time when the images are taken. If an image meeted the following judgemental standards with a mesh, the mesh is evaluated as covered by the image. It is assumed that the center of the mesh \mathbf{m} , the normal vector of the mesh \mathbf{n} , the position of the camera \mathbf{p} , the camera's central axis vector \mathbf{c} , and the eye vector \mathbf{r} , which is a vector from the camera to the mesh. :

- [a] The image is shot in a normal way.
- [b] Direct distance: $d = |\mathbf{m} - \mathbf{p}| < d_{\max}$ (① in Fig.3)
- [c] Position in the image: $|\frac{c_z}{c_x}| < h_{\max} \cap |\frac{c_y}{c_x}| < v_{\max}$ (② in Fig.3) ,where the center of the mesh in the camera coordinates is given by (c_x, c_y, c_z) .
- [d] Angular difference: $|\frac{\mathbf{n} \cdot \mathbf{c}}{|\mathbf{n}| |\mathbf{c}|}| > s_{\min}$ (③ in Fig.3)
- [e] The mesh is not occluded by other meshes(④ in Fig.3). Meshes near by \mathbf{r} are figured out if it occludes \mathbf{r} one by one. The judgement of the mesh k is described as follows:
 - 1) Calculate the point \mathbf{i} , the intersection of the plane defined by mesh k and \mathbf{r} .
 - 2) If the intersection point \mathbf{i} is inside the mesh k , the mesh is judged to be occluded by the mesh k : Let $\mathbf{n1}_k = \mathbf{v1}_k - \mathbf{i}$, $\mathbf{n2}_k = \mathbf{v2}_k - \mathbf{i}$, $\mathbf{n3}_k = \mathbf{v3}_k - \mathbf{i}$. If the signs of $\mathbf{n1}_k \times \mathbf{n2}_k$, $\mathbf{n2}_k \times \mathbf{n3}_k$, and $\mathbf{n3}_k \times \mathbf{n1}_k$ are the same, \mathbf{i} is within the triangle, where $\mathbf{v1}_k$, $\mathbf{v2}_k$, and $\mathbf{v3}_k$ are vertices of the mesh k .

IV. PATH PLANNING

The purpose of this method is to generate a low-cost path which can observe the uncovered meshes revealed by the mesh evaluation. In order to meet the limited computational budget of AUVs, the method generates not an optimized solution but an executable and approximate solution. The path is defined as a set of way points which consist of a horizontal position

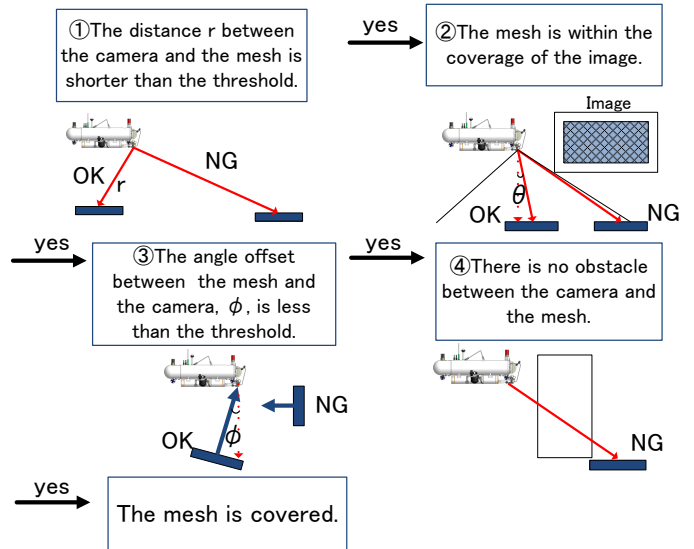


Fig. 3. Outline of mesh evaluation

(x, y), depth z , and heading ψ . Fig.4 shows the outline of the path planning. First, all of the uncovered meshes are split into groups by their positions. Then the groups are omitted if their area are smaller than a threshold (① in Fig.4). After that ,the path is generated for each group (② in Fig.4). Then the order of the groups are decided (③ in Fig.4). At last path is improved by changing the order of the waypoints (④ in Fig.4).

A. Path generation in each group(② in Fig.4)

First view points which can cover the uncovered meshes are calculated. Then the path which pass the view points in an efficient way is generated. At last, way points, the position of the AUV, are decided.

B. Calculate a view point for each meshes(②-A in Fig.4)

First of all, the suitable view point, $p_i(x_i, y_i, z_i, \psi_i)$, is decided for each uncovered mesh $M_i(x_i^m, y_i^m, z_i^m)$. The requirements for view points to fulfill are following things:

- The mesh is projected to the center of the image.
- The distance from the mesh and the view points is D , which is decided in advance.
- The image meets requirement d and e in Section III-B.

As an example, consider the case the AUV has two cameras. One is for looking forward, the other is for downward. As the orientation is not restricted when the view point is for downward looking camera, the view point for the downward camera has flexibility. As a consequence the view points for the downward camera take priority because the shorter path is expected. If a view point for the downward camera is not found, a view point for the forward camera is searched. If a view point for the forward camera is not also found, the mesh is regarded as inability to be observed. View points for

forward looking camera is calculated as follows:

$$x_i = x_i - D' \cos \phi \quad (1)$$

$$y_i = y_i - D' \sin \phi \quad (2)$$

$$z_i = z_i^m + D \sin(c_a) \quad (3)$$

$$\psi_i = -\frac{|m_x|}{m_x} \arctan \frac{m_y}{m_x} \quad (4)$$

$$D' = D \cos(c_a) \quad (5)$$

It is assumed that (m_x, m_y, m_z) is the component of the normal vector of M_i , and c_a is the pitch angle of the camera.

C. Screen view points(②-B in Fig.4)

The selection criterion of view points is to minimize view points and to maximize the uncovered mesh which is covered by the view points. Algorithm 1 shows the way of screening the view points. Let $s_{ij} = \text{evaluate}(i, j)$ denote the function that returns 1 if the uncovered mesh M_j is covered by the view point p_i otherwise returns 0. The judgemental standard is same as section III-B. Let $t_i = \sum_j^n s_{ij}$, the number of meshes which the view point p_i can cover. Let N denote the number of uncovered meshes. It is assumed that a view point should cover at least M meshes.

D. Generate path(②-C in Fig.4)

Next, path planning in each group is executed. In fact the method is to decide the order of the view points which is screened in section IV-C and then to generate the way point for each view points. c_{ij} , moving cost from the way point w_i to w_j is defined as $a_{ij} + Wb_{ij}$. Let a_{ij} denote the vertical distance from w_i to w_j , and b_{ij} the angles the AUV turns at w_j . W is a constant term depending on the relationship between the turning speed and forward movement speed. The solution of this problem is as follows:

- 1) The initial point is the farthest point from the center of the group.
- 2) The nearest point from the present point which is not passed yet is decided as the next point.
- 3) After repeating 2, calculation is terminated if all points are passed.

E. Group ordering(③ in Fig.4)

Then the groups are ordered. Only the start points and the last points for each groups are used for calculation for saving calculation amount. The solution of this problem is as follows:

- 1) The initial point is the present location of the AUV.
- 2) The group of which start point is nearest start point from the present point (the goal point of the present group) which is not passed yet is decided as the next group.
- 3) After repeating 2, calculation is terminated if all groups are passed.

F. Path improvement(④ in Fig.4)

At last, path is improved in consideration of computational complexity. If the number of way points is beyond threshold, shortest path search is executed. Otherwise, the path is improved by 3-opt method.

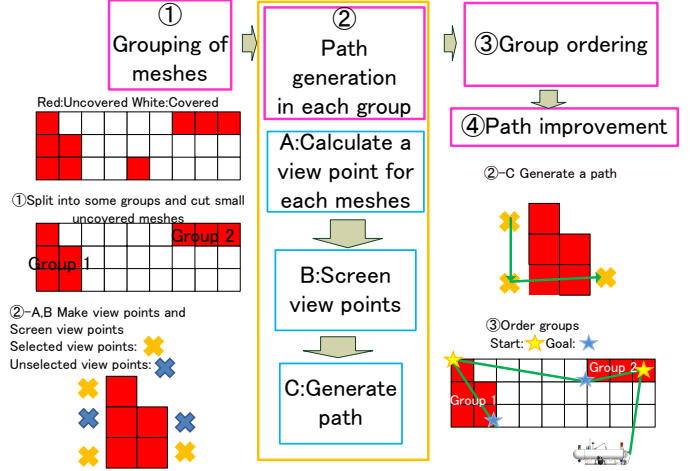


Fig. 4. Outline of path planning

Algorithm 1 Screen view points

```

# Initialization
for i = 0 to N - 1 do
    for j = 0 to N - 1 do
        sij = evaluate(i, j)
    end for
end for
for i = 0 to N - 1 do
    ti = 0
    for j = 0 to N - 1 do
        ti += sij
    end for
end for
# Screen view points
while max(t) > M do
    k = argmaxi(ti)
    Select k as view point
    for i = 0 to N - 1 do
        for j = 0 to N - 1 do
            sij = (1 - skj)sij
        end for
    end for
    for i = 0 to N - 1 do
        ti = 0
        for j = 0 to N - 1 do
            ti += sij
        end for
    end for
end while

```

V. POST PROCESSING

Mesh evaluation method is used for the judgement whether the AUV observed the mesh or not on site. So even if some images covers the mesh, the evaluation end with the first image which cover the mesh. However the best image must be found when the 3D map is made in post processing. The way of choosing best image for each mesh is to evaluate quality q for each images. q is evaluated by the same way as section III-B and described using the sign of section III-B as below.

$$q = \kappa \left(3 - \frac{d}{d_{max}} - \frac{|cz_g|}{|cx_g|} - \frac{|cy_g|}{|cx_g|} + \frac{\mathbf{n} \times \mathbf{c}}{|\mathbf{n}| |\mathbf{c}|} \right) \quad (6)$$

Let $\kappa = 1$ when there is no obstacle between the camera and the mesh otherwise $\kappa = 0$. The constant term is set for the purpose of setting q to be plus sign. The parameter can be used weighting factor, but in this time these are the same weight.

VI. TANK EXPERIMENT

The demonstration experiment was held in IIS Ocean Engineering Basin [7] on December 2012.

The following is the experimental procedure.

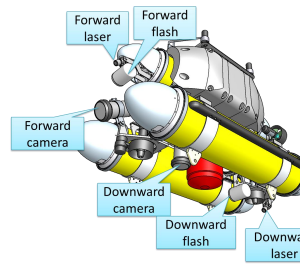
- Initial observation phase
 - The AUV observes the floor by following pre-determined path.
 - The AUV controls altitude as 2.0 m.
- Calculation phase
 - The AUV generates a new path base on the information obtained during the initial observation phase.
 - The AUV controls itself still.
- Re-observation phase
 - The AUV observes the floor by following the new path.

A. AUV Tri-TON

The AUV Tri-TON [8] was used for the experiment. Tri-TON was developed by Institute of Industrial Science, the University of Tokyo in 2011. Table.I shows the specification of the AUV. The positioning scheme uses a Doppler Velocity Log (DVL) and Fiber Optic Gyro (FOG). The control uses proportional integral derivative controller. For vertical control, the AUV can control altitude and depth. For horizontal control, the AUV can control speed by DVL. For orientation control, the AUV can control orientation and angular speed by FOG. Fig.5 shows the specification of the cameras. Table.II shows the experimental setup of the AUV. The AUV has a light-section ranging system consisting of cameras and sheet lasers to profile seafloor with sub-centimeter resolution. The sensor pose (three-dimensional position and orientation) at each moment of data acquisition is cashed in the memory of the AUV.

TABLE I
SPECIFICATION OF THE AUV TRI-TON

Size	1.4m(L) \times 0.75m(H) \times 0.6m(W)
Mass	229.4kg
Max.depth	800m
Duration	10 hours
Computer	Pico820 x 2(Intel Atom 1.60GHz)
Thrusters	2 (Surge) 2(Heave) 1(Sway)



Camera model	Lumenera USB Camera Lu165
Resolution[pixel]	1392 pixel \times 1040 pixel
View angle of forward camera (in water)	64.4 deg \times 50.4 deg
View angle in of downward camera (in water)	66.0 deg \times 51.8 deg
Laser model	Greenlyte-MV EXCEL
Laser wavelength	532nm
Laser illuminating angle (in water)	67 deg
Flash light GN	12
Flash illuminating angle (in water)	80 deg \times 90 deg

Fig. 5. AUV Tri-TON and the specification of the cameras

B. Experiment

Fig.6 shows the experimental setup. The red dot represents the start point and the lines represent robot coordinate. The initial way points are shown in Fig.7. The experimental conditions are set like below to avoid the AUV from bumping the wall or floor:

- The altitude of the AUV is above 1.0 m and below 3.5 m.
- The x position of the AUV is above 0 m and below 12 m.
- The y position of the AUV is above -3.4 m and below 3.4 m.

The relative position of the targets is shown in Fig.8. Fig.9 shows the specification of the targets.

VII. RESULTS

TABLE II
EXPERIMENTAL SETUP OF THE AUV TRI-TON

Surge velocity	10 cm/s
Sampling cycle (terrain)	1 s
Sampling cycle (image)	10 s
Depression angle of forward camera	-13.2 deg
Depression angle of forward laser	-25.5 deg
Depression angle of downward camera	-90 deg
Depression angle of downward laser	-63.7 deg

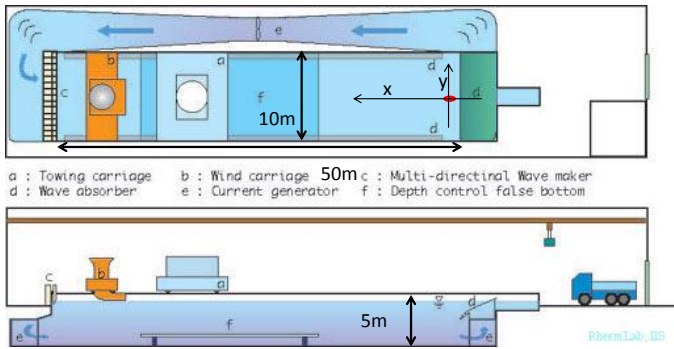


Fig. 6. Tank and start point [7]

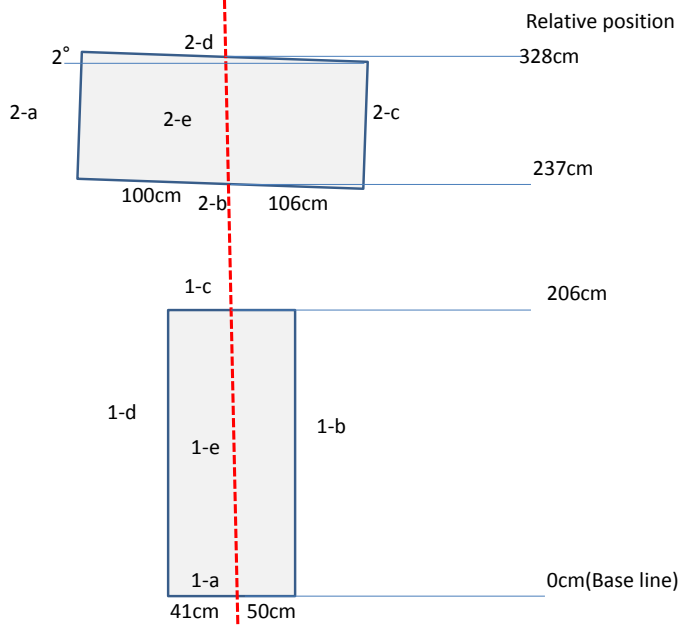


Fig. 8. Relative position of the targets

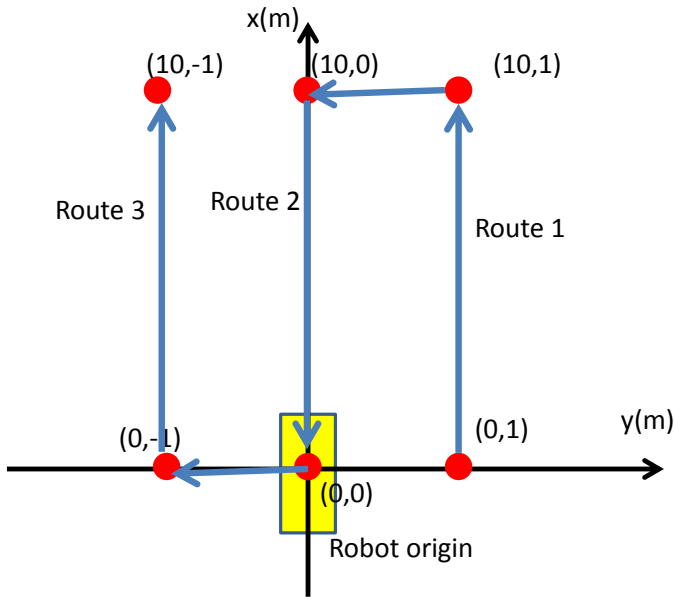


Fig. 7. Initial way points

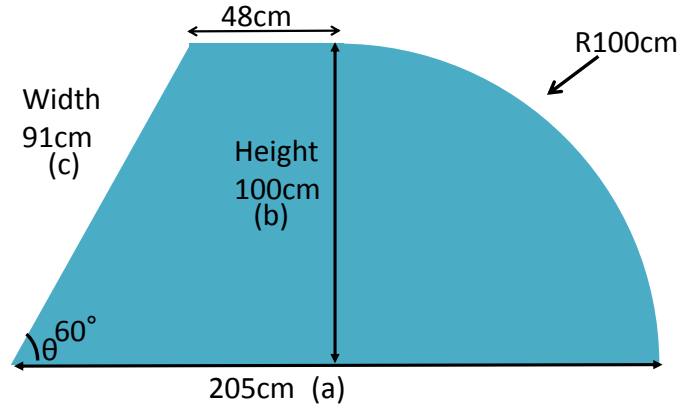


Fig. 9. The specification of the targets

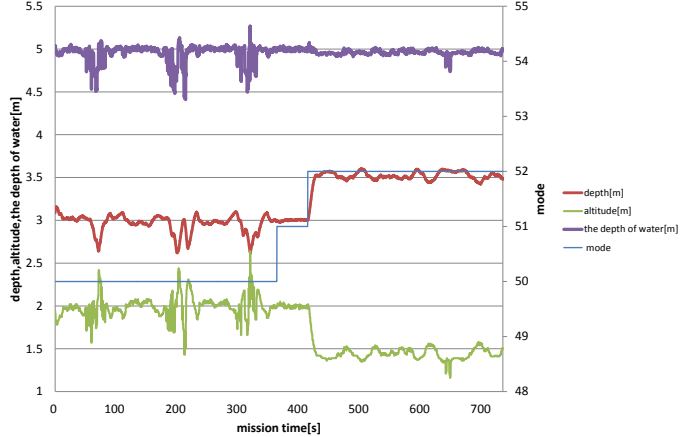


Fig. 10. Observed depth and altitude

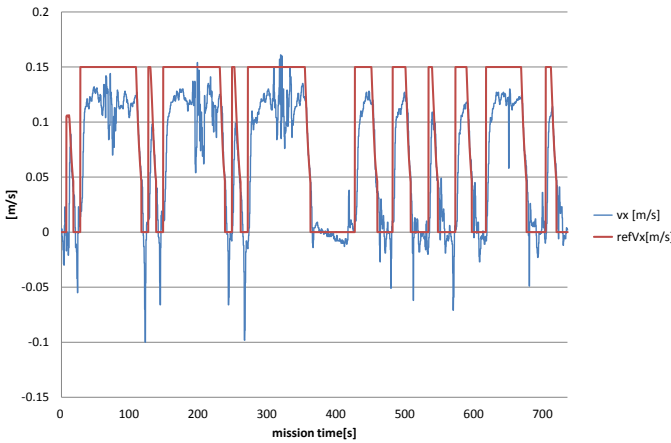


Fig. 11. Observed speed of x and the command value

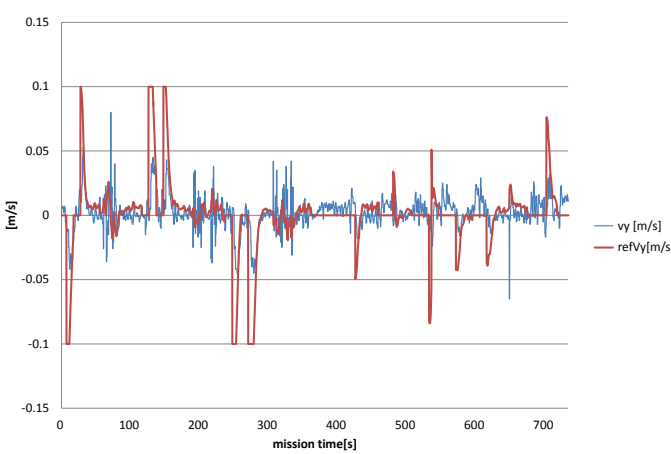


Fig. 12. Observed speed of y and the command value

Fig.10 shows the depth and the altitude of the AUV. Mode 50 means the initial observation phase, 51 means the calculation phase and 52 means the re-observation phase. Fig.11 shows the speed of x and the command value. vx represents the speed of x and refVx represents the command value. Fig.12 shows the speed of y and the command value. vy represents the speed of y and refVy represents the command value. Fig.13 shows yaw angle and the command value. yaw represents the yaw angle and refVa represents the command value. The vehicle is designed to stable at roll and pitch and dose not control them.

TABLE III
THE MEASUREMENTS BEFORE DENOISING

Parameter	ground truth	measurements
Length of the target (a) [cm]	205	204
Length of the target (b) [cm]	100	99
Length of the target (c) [cm]	91	97
θ [degree]	60	62
Length of the gap between target 1 and 2 [cm]	31	19
Vertical distance from floor [cm]	495	492

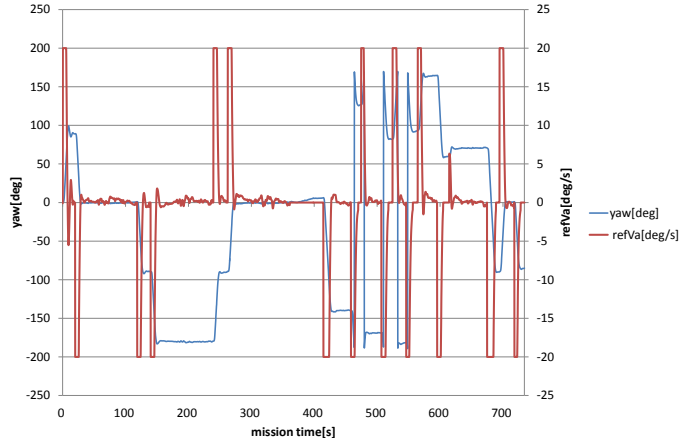


Fig. 13. Observed yaw and the command value

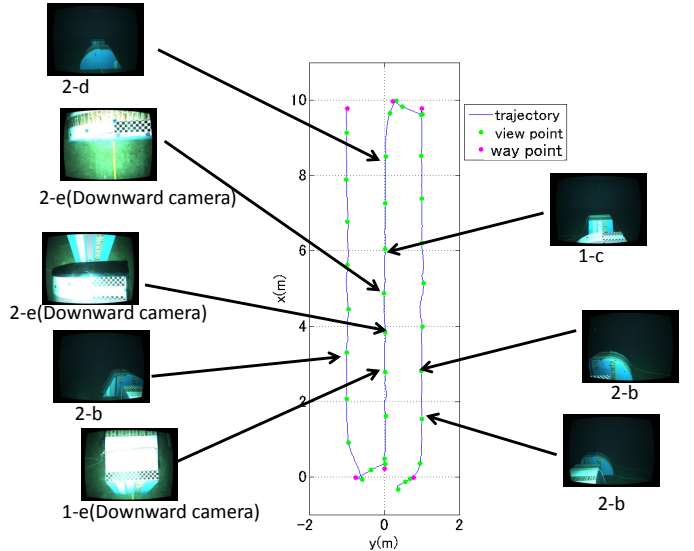


Fig. 14. Trajectory of initial observation phase

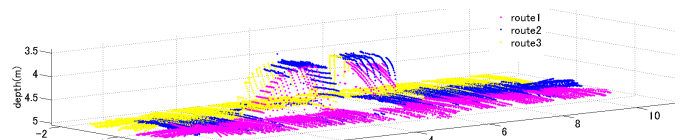


Fig. 15. Results of the terrain measurement before denoising

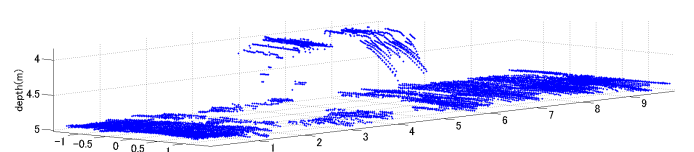


Fig. 16. Results of the terrain measurement after denoising

TABLE IV
THE MEASUREMENTS AFTER DENOISING

Parameter	ground truth	measurements
Length of the target (a) [cm]	205	204
Length of the target (b) [cm]	100	99
Length of the target (c) [cm]	91	—
θ [degree]	60	—
Length of the gap between target 1 and 2 [cm]	31	31
Vertical distance from floor [cm]	495	492



Fig. 17. Images of the forward camera taken at the initial observation phase

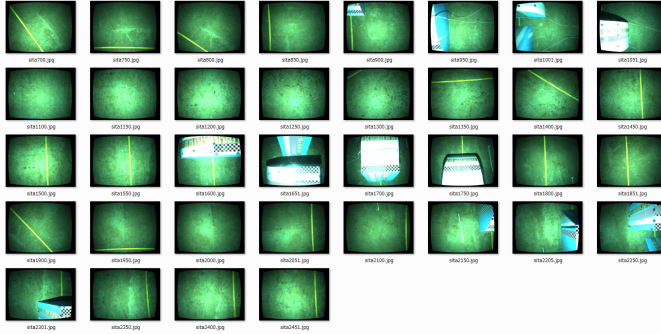


Fig. 18. Images of the downward camera taken at the initial observation phase

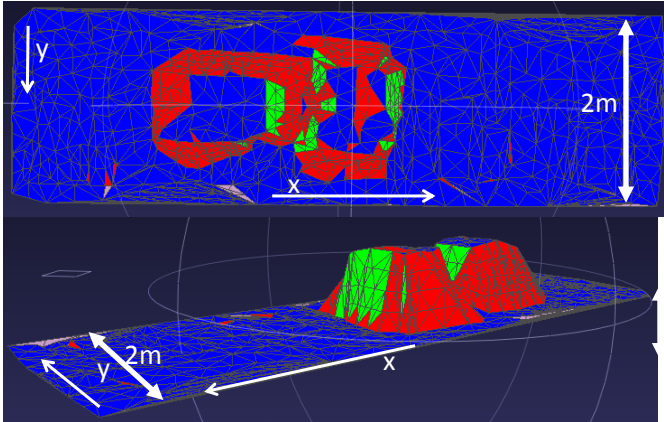


Fig. 19. Results of mesh evaluation after initial observation Blue: covered by the downward camera Green: by the forward one Red: uncovered

TABLE V
CALCULATED WAY POINTS

waypoint	x[m]	y[m]	depth[m]	yaw[deg]
1	7.1	-2.9	4.0	123.9
2	4.5	-3.4	4.0	80.8
3	3.5	-3.4	4.0	90.0
4	1.3	-2.8	3.9	57.1
5	3.4	3.4	4.5	268.7
6	5.0	3.5	4.4	272.4

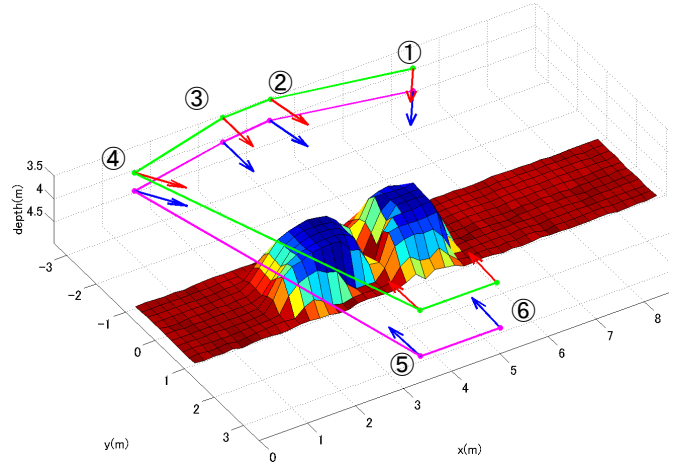


Fig. 20. Calculated way points and actual way points

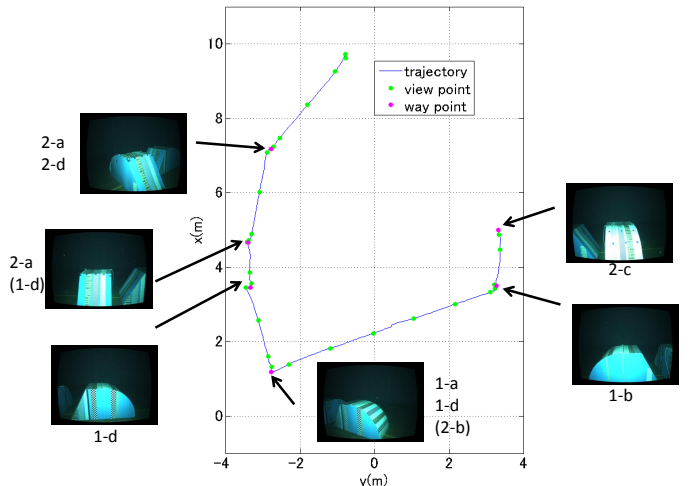


Fig. 21. Trajectory of re-observation phase

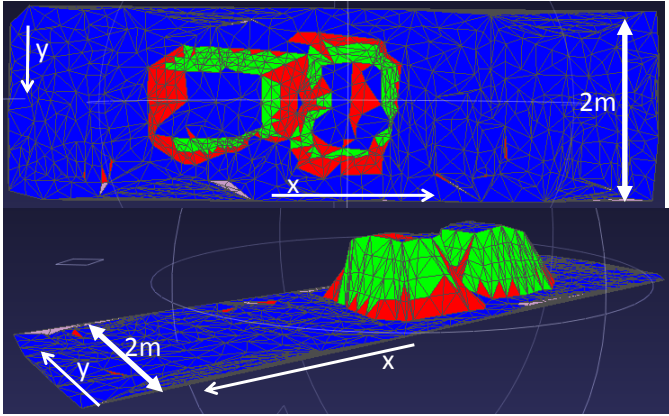


Fig. 22. Results of mesh evaluation after re-observation phase

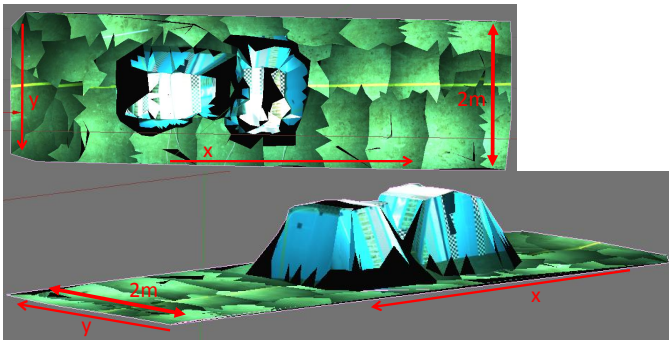


Fig. 23. Texture mapping results obtained by mesh evaluation

Fig.14 shows the trajectory and images of the initial observation phase. The terrain measurement results before denoising is shown in Fig. 15 and Table. III. The pink dots is measured at the route 1, the blue at the route 2 and the yellow at the route 3. The terrain measurement results after denoising is shown in Fig. 16 and Table. reftb:ad. Because of the threshold of the denoising is too tight, the surface of the wall disappeared partly. Fig.17 and 18 shows the images taken at the initial observation phase. The results of the mesh eval-

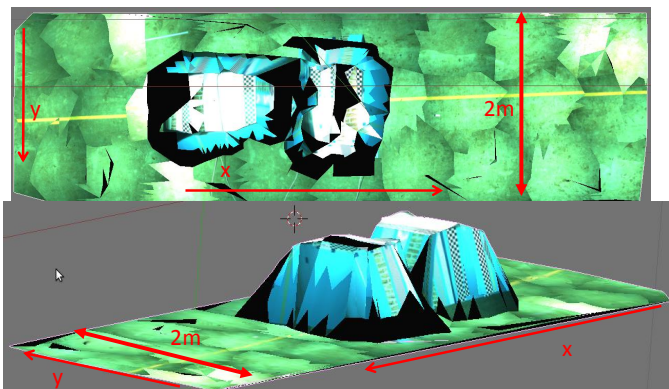


Fig. 24. Texture mapping results obtained by post processing

uation is shown in Fig. 19. The blue mesh is covered by the downward camera. The green mesh is covered by the forward camera. The red mesh is not covered yet. Henceforth in this paper the color coding is used. The parameter is set as $d_{max} = 4000[\text{mm}]h_{max} = 0.47v_{max} = 0.38s_{min} = 0.71(45[\text{deg}])$. The coverage ratio is defined as the proportion of the area of covered meshes to the area of all meshes. The coverage ratio of the initial observation phase is 0.73. The coverage ratio of the forward camera is 0.06. Fig. 20 and Table. V shows the calculated way points. Blue arrows and pink line represents calculated way points and path. Red arrows and green line represents actual considering the experimental procedure. Fig. 21 shows the trajectory and the images taken at the re-observation phase. Texture mapping results obtained by the mesh evaluation is shown in Fig. 23. Texture mapping results obtained by post processing is shown in Fig. 24.

VIII. DISCUSSION

Required time for calculation phase was 50 seconds. It is short enough to use for actual use.

The uncovered wall are shot at all of the way points of re-observation phase. The coverage ratio after re-observation phase is 0.82 and the ratio of forward camera is 0.15. There are mainly three reasons the remaining 0.18 occurs.

First, the actual way points restricted by the experimental conditions cannot cover the lower part of the targets. In the simulation the calculated way points are used for the re-observation. In this case, coverage ratio is 0.88 and the ratio of forward camera is 0.202.

Second, overmuch denoising causes the wrong awkward mesh. The mesh is more difficult to cover than the real. If denoising perform well, the coverage ratio after initial observation is 0.70 and the ratio of forward camera is 0.051. The ratio after re-observation is 0.85 and the ratio of forward camera is 0.196.

Last, The threshold of screening view points, M in section IV-C, is too high. If the threshold of screening view points changes lower, the way points increase. In the experiment M is set as 15, in the simulation M is set as 6. In the case, coverage ratio after re-observation is 0.92 and the ratio of forward camera is 0.243. Table.VI shows the coverage ratio of all cases. If the threshold of screening view points is set lower than 6, the coverage ratio will be higher. However the cost to complete re-observation will be higher too. So the threshold should be decided by considering purpose, action time, and size of the target area.

Fig.24 is bright as compared to Fig.23. It is because the image is better if the distance between the mesh and the camera is nearer.

IX. CONCLUSION

The authors proposes the method for 3D image mapping by AUVs by generating 3D mesh, evaluating meshes and planning new path. The performance of the method was verified by the tank experiment by AUV Tri-TON. However, in order to perform this method, it is necessary to change the threshold

TABLE VI
COVERAGE RATIO

Method	phase	Coverage ratio	Coverage ratio of forward camera
Original	initial	0.73	0.06
	re-observation	0.82	0.16
	simulation	0.88	0.20
denoising	initial	0.70	0.05
	re-observation	0.85	0.20
screening	re-observation	0.92	0.24

value for the mesh evaluation and path generation to fit the purpose and the terrain of the mission. If the density of terrain measurement is also evaluated and integrate into the path planning, the obtained results would become precise. The previous work is done about evaluating the density of terrain measurement [9], [10]. By using this method, AUVs can obtain a full-coverage 3D image of seafloor with single deployment.

ACKNOWLEDGMENT

This work was supported by MEXT.

REFERENCES

- [1] Matthew Johnson-Roberson, Oscar Pizarro, Stefan B. Williams, and Ian Mahon. Generation and visualization of large-scale three-dimensional reconstructions from underwater robotic surveys. *J. Field Robot.*, 27(1):21–51, 2010.
- [2] Michael Jakuba, Stefan B. Williams, Oscar Pizarro and Neville Barrett. Auv benthic habitat mapping in south eastern tasmania. *FSR 2009*, 2009.
- [3] Toshihiro Maki, Ayaka Kume, and Tamaki Ura. Volumetric mapping of tubeworm colonies in kagoshima bay through autonomous robotic surveys. *Deep Sea Research Part I: Oceanographic Research Papers*, 58:757–767, 2011.
- [4] X. Sun, P.L. Rosin, R.R. Martin, and F.C. Langbein. Fast and effective feature-preserving mesh denoising. *IEEE Trans. Visualization and Computer Graphics*, 13(5):925–938, 2007.
- [5] Markus Gross and Hanspeter Pfister, editors. *Point-Based Graphics*. Morgan Kaufmann, 2007.
- [6] Michael Garland and Paul S. Heckbert. Surface simplification using quadric error metrics. In *Computer Graphics(Proc.SIGGRAPH 97)*, pages 209–216. ACM, 1997.
- [7] Iis ocean engineering basin. <http://seasat.iis.u-tokyo.ac.jp/rheem/iiisoeb.html>.
- [8] Toshihiro maki et al. Development of an autonomous system for 3d mapping of hydrothermal vent fields. In *The 22nd Ocean Engineering Symposium*, 2011.
- [9] Paul S. Blaer and Peter K. Allen. View planning and automated data acquisition for three-dimensional modeling of complex sites. *J. Field Robot.*, 26:865–891, November 2009.
- [10] Geoffrey A. Hollinger, Urbashi Mitra, and Gaurav S. Sukhatme. Active classification: Theory and application to underwater inspection. *CoRR*, abs/1106.5829, 2011.